frontiers in Earth Science

ORIGINAL RESEARCH
published: 12 October 2021
doi: 10.3389/feart.2021.760216

Color Reflectance of Coastal Sediments in the South Bohai Sea and its Implication to Orbital Forcing of East Asian Summer Monsoon

Yibing Li[1], *Yanping Chen*[2], *Xingyu Jiang*[3] *and Liang Yi*[1]*

[1]State Key Laboratory of Marine Geology, Tongji University, Shanghai, China, [2]Second Institute of Oceanography, Ministry of Natural Resources, Hangzhou, China, [3]Key Laboratory of Muddy Coastal Geo-Environment, Tianjin Centre, China Geological Survey, Tianjin, China

There are two distinct variabilities of the East Asian summer monsoon (EASM) on orbital timescales observed in different proxies, and the forcing mechanisms between them are hotly debated. One of the ways to reconcile the debate is to present a geological archive recording two cycles in dominance and somehow in equivalence. In this work, we retrieved an EASM record by studying color reflectance of coastal sediments in the south Bohai Sea, East Asia. The leading component of reflectance derivative spectra accounts for 58.9% variance in total and its loading spectrum can be well correlated to that of mineral assemblages of illite and goethite. For this monsoonal record, orbital variabilities in precession and eccentricity bands are highlighted. By comparing this monsoonal record to previously published proxies, it is speculated that the spectral difference in the sediments of the south Bohai Sea and between various proxies in the EASM domain may indicate an integrated forcing of solar insolation and ice-sheet evolution in the late Quaternary. Overall, the monsoonal record in the Bohai Sea offers an opportunity to fill the gap of the diverse periodicities between various proxies, which is critical to extending our understanding of the EASM on orbital timescales.

Keywords: color reflectance, Bohai Sea, late Quaternary, East Asian summer monsoon, orbital variabilities

OPEN ACCESS

Edited by:
Fangjian Xu,
China University of Petroleum (Huadong), China

Reviewed by:
Zhengguo Shi,
Institute of Earth Environment (CAS), China
Haiwei Zhang,
Xi'an Jiaotong University, China

***Correspondence:**
Liang Yi
yiliang@tongji.edu.cn

Specialty section:
This article was submitted to Marine Geoscience, a section of the journal Frontiers in Earth Science

Received: *17 August 2021*
Accepted: *28 September 2021*
Published: *12 October 2021*

Citation:
Li Y, Chen Y, Jiang X and Yi L (2021) Color Reflectance of Coastal Sediments in the South Bohai Sea and its Implication to Orbital Forcing of East Asian Summer Monsoon. Front. Earth Sci. 9:760216. doi: 10.3389/feart.2021.760216

INTRODUCTION

The Asian Monsoon plays a critical role in transporting large quantities of heat and moisture to the East Asia, the most populated region on the Earth (Zhang et al., 2008; Tan et al., 2021), and their evolution has been attracting a great amount of research attentions from geological records to numerical modeling (Jiang and Lang, 2010; Shi et al., 2012; Wang et al., 2014; An et al., 2015; Shi et al., 2019; Cheng et al., 2021). These geological records include loess deposits (An et al., 2001; Guo et al., 2002; Sun et al., 2019), speleothem records (Wang et al., 2001; Cheng et al., 2009; Cheng et al., 2016), and marine and lacustrine sediments (Tian et al., 2008; An et al., 2011; Clemens et al., 2018; Yi et al., 2018; Chen et al., 2020; Xu et al., 2021). Because of the spectral difference between proxies, the variability and mechanism on orbital timescales are hotly debated, especially for the East Asian summer monsoon (EASM). The most commonly viewpoints can be summarized into two scenarios.

1) The monsoon is interpreted as an inter–tropical convergence zone (ITCZ) substantially away from the equator (Wang, 1994; Chao and Chen, 2001), and the EASM variability is predominated by precessional cycles, i.e., 19–23 kyr (Wang et al., 2008; Cheng et al., 2009; Jo et al., 2014). In this

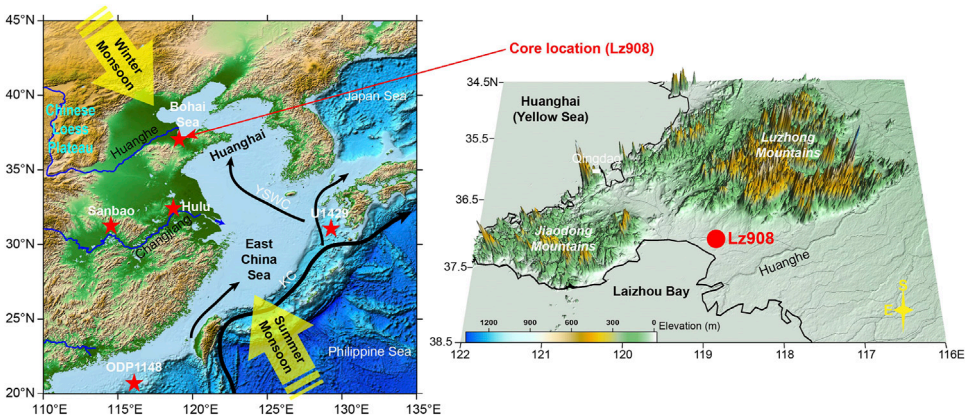

FIGURE 1 | Location, environmental system, and study site (Lz908) and reference sites mentioned in the text. KC, Kuroshio Current; YSWC, Yellow Sea warm current; EASM, East Asian summer monsoon. The base map data was generated using the open and free software DIVA-GIS 7.5 (http://www.diva-gis.org/).

scenario, the EASM is proposed to be directly controlled by solar insolation (Kutzbach, 1981; Ruddiman, 2006), mainly reported in Chinese cave deposits, such as the Hulu and Sanbao caves (**Figure 1**). 2) The EASM variability is predominated by the eccentricity cycle, i.e., 100 kyr, which highlights the role of global ice volume in modulating the thermodynamic difference between the Asian continent and Pacific Ocean (An et al., 1990). In this scenario, the EASM could be controlled by glacial–interglacial alternations (Ding et al., 1994; Ding et al., 1995; Wang, 1999; Guo et al., 2002; Guo et al., 2004), such as profiles in the Chinese loess plateau and ODP 1148 site in the South China Sea (**Figure 1**).

Besides of these two scenarios, the dominant obliquity band in the Chinese loess plateau and non–precession component in the EASM variability in marine sediments at IODP U1429 site are also proposed (Li et al., 2017; Clemens et al., 2018), inferring a more complex response of the EASM to orbital forcing. To reconcile these hypotheses, Cheng et al. (2021) suggested that different archives preferentially record a certain aspect of the EASM and spatial patterns of rainfall and wind across the precession cycle may be the major reason producing distinct regional divergences. However, testifying this new hypothesis is not easy, because the former requires a profile with a multiple dominance of eccentricity, obliquity, and precession cycles, or at least an equilibrium between them, while the later needs a full–cover study in the monsoon domain.

The monsoonal record from the Bohai Sea (**Figure 1**), East Asia may offer such an opportunity to fill the gap between the eccentricity–and precession–dominated monsoon variabilities (Yi et al., 2018). In this study, an investigation was reported based on mineral properties of coastal sediments in core Lz908. A monsoon proxy of the late Quaternary was derived and three astronomical rhythms were observed. By comparing to other monsoon proxies across the East Asia, the different roles of monsoonal heat and moisture in pacing different records were discussed.

MATERIALS AND METHODS

Core Lz908

The Bohai Sea is a semi–enclosed interior continental shelf of the East China Sea (**Figure 1**), with an average water depth of 18 m, and it is connected to the Huanghai Sea by the narrow Bohai Strait. Core Lz908 is located onshore near the southern coast of the Bohai Sea (37°09′N, 118°58′E, elevation 6 m). The core was drilled to a depth of 101.3 m with an average recovery rate of 75% in the summer of 2007, by the First Institute of Oceanography, Ministry of Natural Resources of China. The drill site was submerged until the middle of the 20th century.

The upper 54.3 m of the core contains marine and coastal sediments (**Figure 2**), and has been chosen for paleoenvironmental studies (Yi et al., 2012a; Yi et al., 2012b). Integrated the radiocarbon and luminescence–based age model, the geochronology of core Lz908 was established by synchronously tuning sediment grain–size index to the July insolation at 65°N (Yi et al., 2012a), and the tuning bottom (260 ka) has been well constrained by magnetostratigraphy (Yi et al., 2015). Based on this age model (**Figure 2**), the core was sampled in 10–cm interval to investigate mineral properties of coastal sediments in the south Bohai Sea.

Mineralogy by Diffuse Spectral Reflectance

The CIELAB color space, in which any sediment's color can be expressed by L*a*b* values, can provide useful stratigraphic information (Ortiz, 2011; Sun et al., 2011; Yi et al., 2016). Measurements of diffuse spectral reflectance (DSR) were collected at 10–cm resolution (373 samples in total) in the State Key Laboratory of Marine Geology, Tongji University of China. To reduce uncertainties of water losses, the samples of core Lz908 were dried, ground, and compacted before the measurement. The instrument is the Minolta CM–700d spectrophotometer (400–700 nm wavelength range; 10 nm resolution; 3 mm spot size).

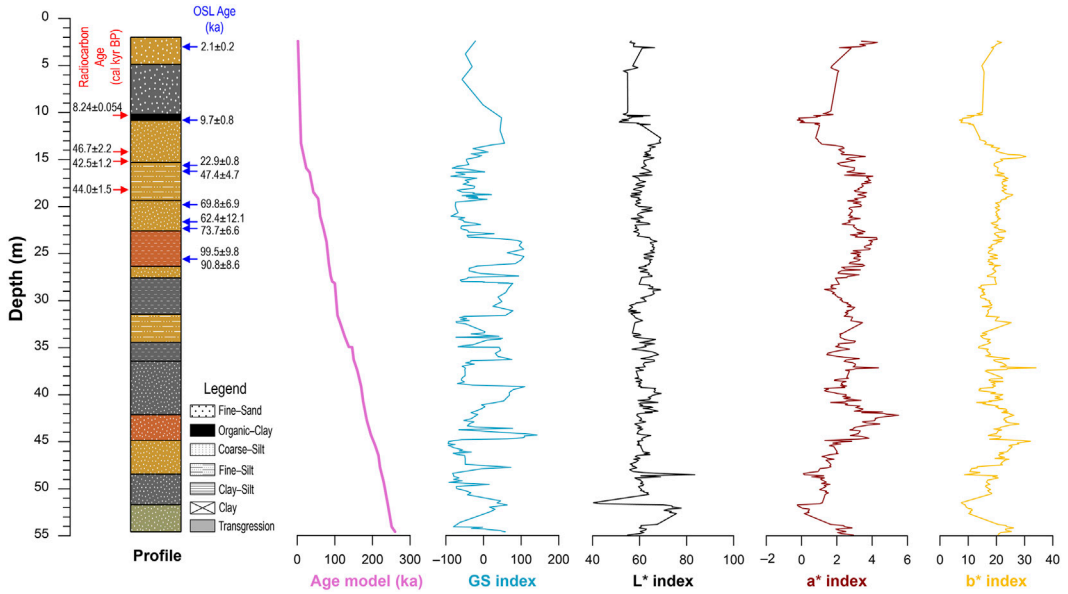

FIGURE 2 | Profile with dating results and age model of core Lz908 (Yi et al., 2012a), changes in sediment grain size (GS index), and color indices (L*a*b*) in the CIELAB color space. L*, lightness; a*, redness (+)/greenness (–); b*, yellowness (+)/blueness (–).

In order to reduce uncertainties of paleoenvironmental inference using original color data (L*a*b*) in such a dynamic region (Yi et al., 2016), we employ principle component analysis (PCA) to identify the contribution of different mineral assemblages to the downcore color variations. The PCA was calculated using the correlation matrix of the center–weighted derivatives of the DSR data (Ortiz et al., 2004; Ortiz, 2011) from core Lz908.

Mineralogy by X–Ray Diffraction

As suggested in previous studies (Ortiz, 2011; Sun et al., 2011; Yi et al., 2016), the results of X–Ray Diffraction (XRD) of the sediments can provide an independent check for the DSR–based mineral identification. Thus, four representative samples from core Lz908 (15, 25, 35, and 45 m in depth) were measured by the XRD, according to the methods described by Liu et al. (2004) as follows.

The XRD clay mineral study was carried out on the <2 μm fraction, which was separated by conventional Stokes' settling after the removal of carbonate and organic matter by acetic acid (15%) and hydrogen peroxide (10%), respectively. Clay minerals were then identified by using an X'Pert PRO, PANalytical XRD instrument (40 kV and 40 mA) at the First Institute of Oceanography, Ministry of Natural Resources of China. Identification of clay minerals was made according to the position of the (001) series of basal reflections observed on the XRD diagrams (Moore and Reynolds, 1997).

RESULTS

The blue–yellow contrast (b*) and the red–green contrast (a*) of the sediments of core Lz908 are closely correlated ($r = 0.72$, $p < 0.01$). The two indices vary between values of −0.24–5.50 and 6.93–34.02, respectively. Sediment brightness (L*) oscillates between values of 51.37–69.16, and its variability became larger below ~48.0 m (**Figure 2**). Changes in the color indices are somehow similar, and extracting the same pattern is a common way for paleoenvironmental inferences.

The PCA results show that the first leading DSR component (CF–1) accounts for 58.9% of the variance in the correlation matrix of the reflectance derivative spectra. To identify the minerals or mineral assemblages associated with the CF–1, we calculate the linear correlation between the CF–1 and known minerals (**Figure 3A**), which are available online from the USGS Digital Spectral Library. The CF–1 can be correlated to a mixture of illite + goethite ($r = 0.98$, $p < 0.01$), similar to ones of core YDZ–3 from the Huanghe River delta (Yi et al., 2016), close to the study site. The first derivative spectrum for pure goethite has principal peaks at 535 and 435 nm (Deaton and Balsam, 1991), also observed in **Figure 3A** (590–540 and 440 nm). For the other two DSR components, which account for 28.6 and 5.5% variance in total, respectively, inherit the high–frequency oscillation on suborbital and millennial timescales, and thus not discussed in this study.

As an independent check on the DSR analysis, additional results were obtained by XRD analysis from four representative sediment samples (**Figure 3B**). The identified minerals are quartz (20.8–29.0 Å), mixed–layer of illite–quartz (26.5–27.0 Å), illite (8.8–8.9 Å, 17.6–17.8 Å), smectite (4.6–4.9 Å), chlorite (6.1–6.3 Å, 18.7–18.9 Å), and mixed–layers of kaolinite–chlorite (12.2–12.5 Å, 24.8–25.3 Å). The result of the XRD–based clay mineral analysis supports the DSR results in this study.

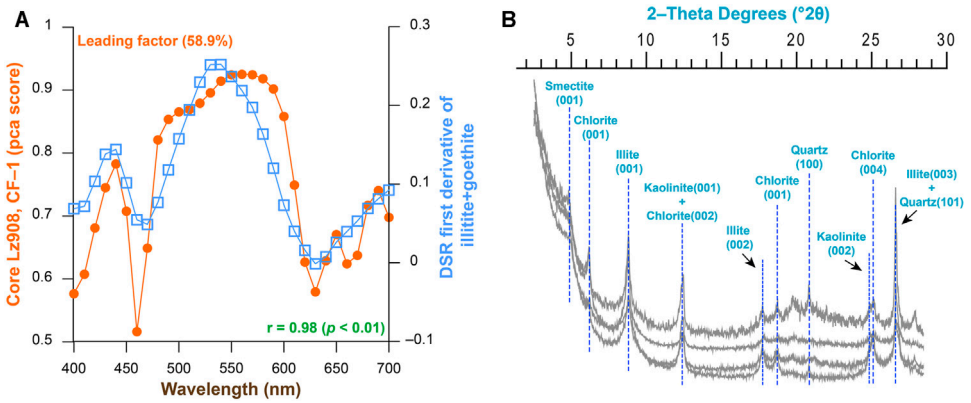

FIGURE 3 | (A) Varimax–rotated factor loadings of core Lz908 and DSR first derivates of mineral standards (Illitite + Goethite) plotted as a function of wavelength; **(B)** Four representative samples for XRD analysis with the identified minerals.

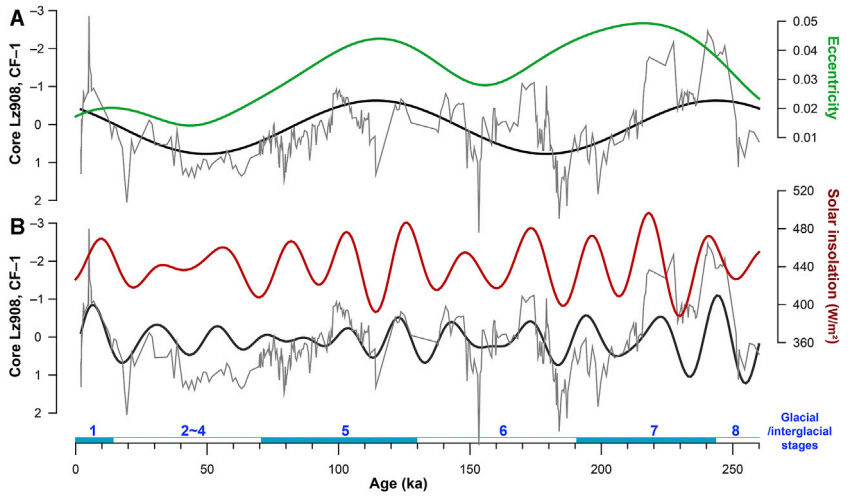

FIGURE 4 | (A) Changes in color (CF–1) index of core Lz908 (thin line) with low–frequent passed variabilities (bold line; FFT filter, < 1/0.0125), *versus* Earth's orbital eccentricity (Berger and Loutre, 1991); **(B)** Changes in color index of core Lz908 (thin line) with precession–band passed variabilities (bold line; FFT filter, 1/0.0255 ~ 1/0.0235), *versus* changes in summer (July 21st) solar insolation at 65°N (Berger and Loutre, 1991).

For the down–core variation, the CF–1 changed cyclically in the late Quaternary, and the most evident variation is the difference between glacial and interglacial intervals. For example, during the last and the penultimate glacial intervals, the illite + goethite content was relatively high (**Figure 4A**). The CF–1 is also characterized in precession bands, and during each interval with high solar insolation, the illite + goethite content was relatively low (**Figure 4B**).

Spectral analysis by the Blackman–Tukey method (Howell et al., 2006) confirms orbital variabilities (**Figure 5A**). As shown, three astronomical rhythms are observed: the 100–kyr periodicity is the major cycle in the CF–1 record, the intensity of 41–kyr periodicity is similar to the one of 23–kyr periodicity, and the 19–kyr cycle is much evident than other proxies of the EASM, such as marine and cave deposits (**Figures 5B,C**). Moreover, the eccentricity band in the GS and the obliquity and precession bands in the CF–1 are observed (**Figure 5**), while for other proxies, either 100–kyr or 23–kyr dominated records, only one periodicity is highlighted (**Figure 5B**), or evident (loess-based proxies) during interglacial intervals (e.g., Ma et al., 2017; Sun et al., 2019).

Further analyses of spectral curves by mathematical unmixing using a Gaussian equation provide a quantitative assessment for each astronomical rhythm (**Table 1**). The ratios of three astronomical rhythms are similar between the deep–sea sediment $\delta^{18}O$ record (MIS) and the magnetic susceptibility record of the Yimaguan profile (frequency–dependent data) from the Chinese loess plateau (MSHA), and between July insolation at 65°N (INS) and the stalagmite $\delta^{18}O$ series (CAVE). However, for records derived from the Bohai Sea, the CF–1 is highlighted in the eccentricity band (48%), followed by a close contribution of precession

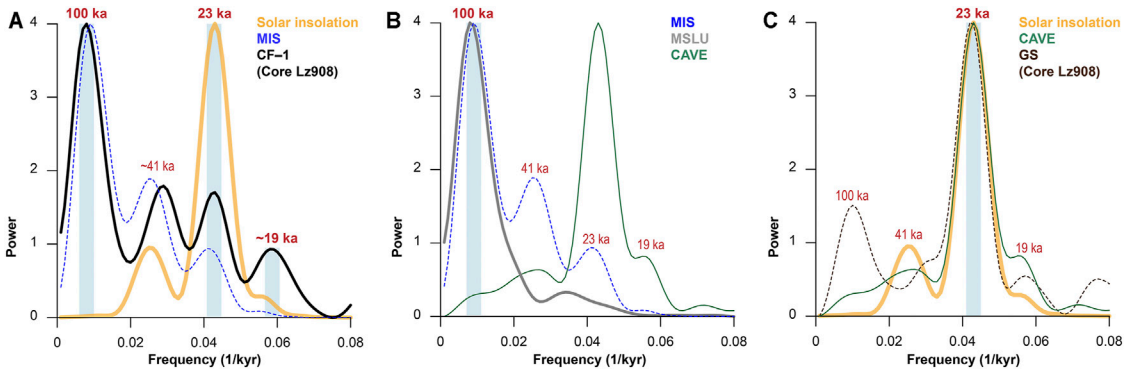

FIGURE 5 | Spectral comparison following the Blackman–Tukey method implemented with the ARAND software package (Howell et al., 2006). MIS, deep–sea sediment $\delta^{18}O$ records (Lisiecki and Raymo, 2005); MSLU, magnetic susceptibility record of the Luochuan profile (low frequency data) from the Chinese loess plateau (Lu and An, 1997); Color (CF–1) and grain–size (GS) indices of core Lz908; INS (solar insolation), July insolation at 65°N (Berger and Loutre, 1991); CAVE, stalagmite $\delta^{18}O$ series (Cheng et al., 2016).

TABLE 1 | Relative ratios of each orbital periodicity in various records.

Proxies	Eccentricity (100 kyr)	Obliquity (41 kyr)	Precession (23 and 19 kyr)
CF–1 (Lz908)	48%	21	21% + 13%
GS (Lz908)	23%	11	58% + 8%
MIS	59%	27	14%
MSHA[a]	59%	24	17%
INS	—	19	77% + 5%
CAVE	5%	11	70% + 14%

[a]*MSHA, magnetic susceptibility record of the Yimaguan profiles (frequency–dependent data) from the Chinese loess plateau (Hao et al., 2012). Other datasets are from* ***Figure 5****.*

components (34%), and the GS is dominated in the precession band (66%), followed by an evident cycle of orbital eccentricity (23%).

DISCUSSION

Monsoonal Proxies of Core Lz908

The sediment grain–size record from the Bohai Sea, namely the GS record of core Lz908, can be used to indicate orbital changes of the EASM in the late Quaternary (Yi et al., 2012a), because the sediment grain–size variation is controlled by river discharge and resuspension process in the tidal zone (Chen et al., 2013; Su et al., 2016). Although the influence of regional sea–level changes on the GS record of core Lz908 cannot be excluded (Yi et al., 2012b), the EASM is the predominant factor controlling sedimentary dynamics in the south Bohai Sea, since ~80% of total variance of the GS record can be explained by solar insolation (Yi et al., 2018).

For the CF–1 record, mineral properties of coastal sediments in the south Bohai Sea are highlighted. Similar because these clay minerals were mainly from the Luzhong Mountains (**Figure 1**), changes in the CF–1 may be linked to weathering processes and river discharge, rather than regional sea–level changes. For example, minerals illite and goethite in the Chinese loess plateau and the Huanghe River delta usually indicate a cold and dry climate in the past (e.g., Ji et al., 2007; Niu et al., 2015). In this study, the low–frequency changes of the CF–1 are in–phase correlated with orbital eccentricity (**Figure 4**), inferring that more illite and goethite were produced during glacial intervals in the Luzhong Mountains. Moreover, regional river inputs usually decrease to a much lower level in winters (Yi et al., 2016), and most of detrital materials are transported to the south Bohai Sea in summers (Yi et al., 2012a), *via* local rivers, such as the Mihe, Xiaoqinghe and Weihe Rivers. Since that the Asian monsoon is the major factor controlling clay minerals in the monsoon domain, such as in the Chinese loess plateau and the Huanghe River delta (e.g., Sun et al., 2011; Zhao et al., 2017; Chen et al., 2021), the in–phase relation between the CF–1 and solar insolation is expected (**Figure 4**). Thus, the CF–1 can be linked to the EASM by mineralogical responses. When the EASM strengthens, a warmer and wetter climate would produce less minerals illite and goethite in the study area; but when the EASM weakens, the CF–1 value increase, indicating more minerals illite and goethite in the sediments.

In summary, there are two monsoonal records derived from core Lz908, and the GS and the CF–1 are linked to the EASM by sedimentary dynamics and mineral properties, respectively (**Figure 6**). In specific, the GS record is correlated with the EASM in the late Quaternary by the processes of sedimentary dynamics and regional rainfall, dominated in precession bands

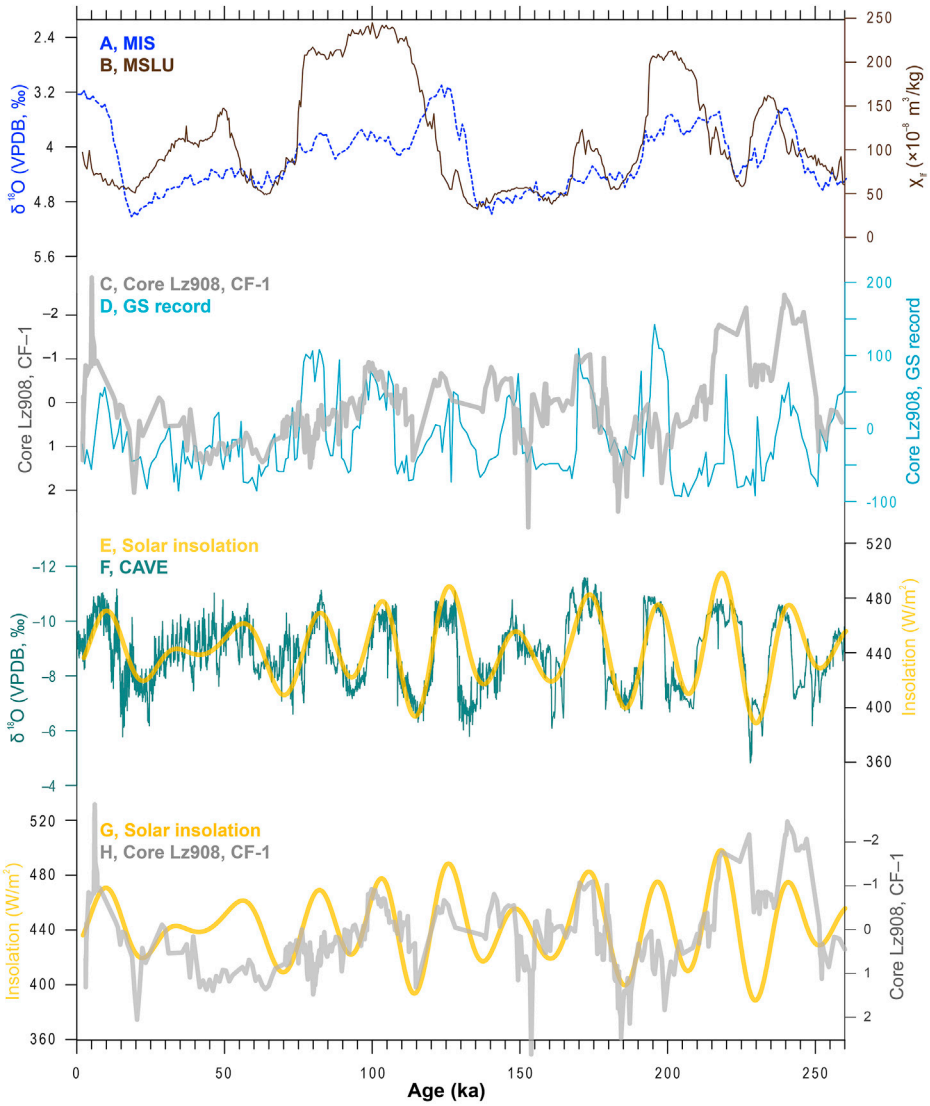

FIGURE 6 | Comparisons between EASM proxies in the late Quaternary. **(A)** MIS record of deep–sea sediment $\delta^{18}O$ (Lisiecki and Raymo, 2005); **(B)** MSLU, magnetic susceptibility record of the Luochuan profile (Lu and An, 1997); **(C–D)** CF–1 and GS records of core Lz908 (this study); **(E)** INS (solar insolation), July insolation at 65°N (Berger and Loutre, 1991); **(F)** CAVE, stalagmite $\delta^{18}O$ series (Cheng et al., 2016). The used datasets were from **Figure 5**.

(**Figure 5C**). By regional weathering and river inputs, the CF–1 record is linked to the EASM through both rainfall and temperature changes, highlighted in eccentricity and precession bands (**Figure 5A**).

An Integrated Forcing

Based on stalagmite records from Hulu, Dongge and Sanbao Caves of China, a clean and dominant precession cycle was observed (e.g., Cheng et al., 2016). In these records, speleothem $\delta^{18}O$ changes can indicate $\delta^{18}O$ variation of local meteoric precipitation and thus characterize the EASM intensity (Yuan et al., 2004; Dykoski et al., 2005; Cheng et al., 2016), which might be largely controlled by the large-scale monsoon circulation and concomitant latitudinal shifts of the monsoon rain belt (Zhang et al., 2021). This relationship leads to the idea that the EASM can be directly driven by solar insolation (Kutzbach, 1981; Zhang et al., 2021), explaining a high similarity in spectral characteristics between the EASM and solar insolation (Jiang and Lang, 2010; Shi et al., 2012; Shi et al., 2019). The linkage involves the shift of the ITCZ location (Wang et al., 2005; Cheng et al., 2009; Jo et al., 2014), which modulates atmospheric circulations (Chao and Chen, 1999) and triggers the onset of Asian monsoon (Chao, 2000). Hence, although the physical significance of stalagmite $\delta^{18}O$ are still hotly debated (Zhang et al., 2019), it is reasonable to speculate that monsoonal moisture is the major factor, since that tropical hydrological cycle varies mainly in precession bands (e.g., Huang et al., 2020) and that summer rainfall can be well constrained by stalagmite $\delta^{18}O$ in the Chinese loess plateau (e.g., Tan et al., 2020).

Loess magnetic susceptibility as a proxy of the EASM is based on pedogenesis and mineral transformation (e.g., Yang et al., 2015), *via* changing rainfall and temperature in the Chinese loess plateau between glacial and interglacial intervals. The monsoon circulation on glacial–interglacial timescales was likely associated to the continental–scale land–sea thermal contrast (Wallace and Hobb, 1977; Webster et al., 1998; Wang and Ding, 2008). Since not all of the rainfall could be used in pedogenesis and because of the loss of evaporation and surface runoff, changes in magnetic susceptibility may reflect effective precipitation (Yi et al., 2018). Changes in global ice volume are proposed to modulate the thermodynamics of land–sea contrast (An et al., 1990), and it is reasonable to speculate that temperature changes were relatively important, considering that pedogenesis and chemical weathering in the Chinese loess plateau are likely not evident when winter temperature is below 0°C (Hao and Guo, 2001). In addition, solar insolation could also modulate the sea-land thermal contrast and this influence was likely evident during interglacial intervals (e.g., Ma et al., 2017).

For the GS record of core Lz908, regional rainfall is the dominant factor (Yi et al., 2012a), while the influence of tropical cyclones (Yi et al., 2018) and sea levels (Yi et al., 2012b) can be excluded, and the former were likely paced by global temperature changes (e.g., Zhou et al., 2019). Because of this, the GS record is dominated by precession cycles with a significant contribution in eccentricity and obliquity bands (**Table 1**). For the CF–1, the intensified monsoon (rainfall) increases regional river discharge (Chen et al., 2021), thus introducing precessional variabilities into the sediments. On the other hand, the intensified monsoon (temperature) may also strengthen regional pedogenesis in the Luzhong Mountains (**Figure 1**), likely resulting in a transit of variabilities of eccentricity and obliquity into the sediments. Because of this, the CF–1 record is dominated by eccentricity cycles with an equivalent component in precession bands (**Table 1**). Hence, monsoonal signals in the Bohai records may be not singly linked to temperature or rainfall changes like the loess–and the speleothem–based proxies, but demonstrate an integrated forcing of ice–sheet evolution and solar insolation.

Overall, although the uncertainties in monsoonal proxies cannot be excluded in this study, the Bohai records likely fill the gap between the new hypothesis of Cheng et al. (2021) and the diverse periodicities of monsoon proxies, supporting that different archives preferentially record a certain aspect of the EASM. Moreover, the difference between the two Bohai records responding to the EASM might highlight a distinct role of precession and eccentricity cycles, which are worth of further investigation in future.

CONCLUSION

By analyzing DSR and XRD of the sediments in the Bohai Sea, mineral properties of core Lz908 in the late Quaternary were studied. Based on a principle component analysis, the leading component accounts for 58.9% variance in total and its loading spectrum can be well correlated to that of mineral assemblages of illite and goethite. A monsoonal record from the studied core was then derived, and orbital variabilities both in precession and eccentricity bands are evident. By comparing this mineral record to various monsoonal proxies, it is speculated that the precession variability in the EASM is mainly related to rainfall, while the eccentricity variability is likely associated with temperature changes. These findings demonstrate an integrated forcing of ice–sheet evolution and solar insolation in the EASM in the late Quaternary. In summary, the Bohai records may fill the gap of the diverse periodicities between various monsoon proxies, supporting that different archives preferentially record a certain aspect of the EASM.

DATA AVAILABILITY STATEMENT

The raw data supporting the conclusion of this article will be made available by the authors, without undue reservation.

AUTHOR CONTRIBUTIONS

Conceptualization, LY; formal analysis, YL, YC, and XJ; original draft preparation, YL; and review and editing, LY. All authors have read and agreed to the published version of the manuscript.

FUNDING

This research was funded by the Natural Science Foundation of Shanghai, grant number 19ZR1459800, the Global Changing and Air–Sea Interaction, grant number GASI–GEOGE–04, and the National Natural Science Foundation of China, grant number 42177422.

ACKNOWLEDGMENTS

We thank Prof. YU Hongjun in the First Institute of Oceanography, Ministry of Natural Resources of China for providing samples for this study.

REFERENCES

An Zhisheng, Z., Liu Tunghseng, T. S., Lu Yanchou, Y. C., Porter, S. C., Kukla, G., Wu Xihao, X. H., et al. (1990). The Long-Term Paleomonsoon Variation Recorded by the Loess-Paleosol Sequence in Central China. *Quat. Int.* 7-8, 91–95. doi:10.1016/1040-6182(90)90042-3

Berger, A., and Loutre, M. F. (1991). Insolation Values for the Climate of the Last 10 Million Years. *Quat. Sci. Rev.* 10, 297–317. doi:10.1016/0277-3791(91)90033-Q

Chao, W. C., and Chen, B. (1999), "Approximate Co-location of Precipitation and Low-Level Westerlies in Tropical Monthly Means," in *Climate Variations*. Denver, CO: American Meteorological Society. .

Chao, W. C., and Chen, B. (2001). The Origin of Monsoons. *J. Atmos. Sci.* 58, 3497–3507. doi:10.1175/1520-0469(2001)058<3497:TOOM>2.0.CO;2

Chao, W. C. (2000). Multiple Quasi Equilibria of the ITCZ and the Origin of Monsoon Onset. *J. Atmos. Sci.* 57, 641–652. doi:10.1175/1520-0469(2000)057<0641:MQEOTI>2.0.CO;2

Chen, G., Yi, L., Chen, S., Huang, H., Liu, Y., Xu, Y., et al. (2013). Partitioning of Grain-Size Components of Estuarine Sediments and Implications for Sediment Transport in Southwestern Laizhou Bay, China. *Chin. J. Ocean. Limnol.* 31, 895–906. doi:10.1007/s00343-013-2304-y

Chen, Y., Li, Y., Lyu, W., Xu, D., Han, X., Fu, T., et al. (2020). A 5000-Year Sedimentary Record of East Asian Winter Monsoon from the Northern Muddy Area of the East China Sea. *Atmosphere* 11, 1376. doi:10.3390/atmos11121376

Chen, Y., Lyu, W., Fu, T., Li, Y., and Yi, L. (2021). Centennial Impacts of the East Asian Summer Monsoon on Holocene Deltaic Evolution of the Huanghe River, China. *Appl. Sci.* 11, 2799. doi:10.3390/app11062799

Cheng, H., Edwards, R. L., Broecker, W. S., Denton, G. H., Kong, X., Wang, Y., et al. (2009). Ice Age Terminations. *Science* 326, 248–252. doi:10.1126/science.1177840

Cheng, H., Edwards, R. L., Sinha, A., Spötl, C., Yi, L., Chen, S., et al. (2016). The Asian Monsoon over the Past 640,000 Years and Ice Age Terminations. *Nature* 534, 640–646. doi:10.1038/nature18591

Cheng, H., Zhang, H., Cai, Y., Shi, Z., Yi, L., Deng, C., et al. (2021). Orbital-scale Asian Summer Monsoon Variations: Paradox and Exploration. *Sci. China Earth Sci.* 64, 529–544. doi:10.1007/s11430-020-9720-y

Clemens, S. C., Holbourn, A., Kubota, Y., Lee, K. E., Liu, Z., Chen, G., et al. (2018). Precession-band Variance Missing from East Asian Monsoon Runoff. *Nat. Commun.* 9, 3364. doi:10.1038/s41467-018-05814-0

Deaton, B. C., and Balsam, W. L. (1991). Visible Spectroscopy; a Rapid Method for Determining Hematite and Goethite Concentration in Geological Materials. *J. Sediment. Res.* 61, 628–632. doi:10.1306/d4267794-2b26-11d7-8648000102c1865d

Ding, Z., Liu, T., Rutter, N. W., Yu, Z., Guo, Z., and Zhu, R. (1995). Ice-Volume Forcing of East Asian Winter Monsoon Variations in the Past 800,000 Years. *Quat. Res.* 44, 149–159. doi:10.1006/qres.1995.1059

Ding, Z., Yu, Z., Rutter, N. W., and Liu, T. (1994). Towards an Orbital Time Scale for Chinese Loess Deposits. *Quat. Sci. Rev.* 13, 39–70. doi:10.1016/0277-3791(94)90124-4

Dykoski, C., Edwards, R., Cheng, H., Yuan, D., Cai, Y., Zhang, M., et al. (2005). A High-Resolution, Absolute-Dated Holocene and Deglacial Asian Monsoon Record from Dongge Cave, China. *Earth Planet. Sci. Lett.* 233, 71–86. doi:10.1016/j.epsl.2005.01.036

Guo, Z., Peng, S., Hao, Q., Biscaye, P. E., An, Z., and Liu, T. S. (2004). Late Miocene? Pliocene Development of Asian Aridification as Recorded in the Red-Earth Formation in Northern China. *Glob. Planet. Change* 41, 135–145. doi:10.1016/j.gloplacha.2004.01.002

Guo, Z. T., Ruddiman, W. F., Hao, Q. Z., Wu, H. B., Qiao, Y. S., Zhu, R. X., et al. (2002). Onset of Asian Desertification by 22 Myr Ago Inferred from Loess Deposits in China. *Nature* 416, 159–163. doi:10.1038/416159a

Hao, Q., and Guo, Z. (2001). Quantitative Measurements on the Paleo-Weathering Intensity of the Loess-Soil Sequences and Implication on Paleomonsoon. *Sci. China Earth Sci.* 31, 520–5528. doi:10.1007/bf02876216

Hao, Q., Wang, L., Oldfield, F., Peng, S., Qin, L., Song, Y., et al. (2012). Delayed Build-Up of Arctic Ice Sheets during 400,000-year Minima in Insolation Variability. *Nature* 490, 393–396. doi:10.1038/nature11493

Howell, P., Pisias, N., Ballance, J., Baughman, J., and Ochs, L. (2006). *ARAND Time-Series Analysis Software*. Providence RI: Brown University

Huang, E., Wang, P., Wang, Y., Yan, M., Tian, J., Li, S., et al. (2020). Dole Effect as a Measurement of the Low-Latitude Hydrological Cycle over the Past 800 Ka. *Sci. Adv.* 6. eaba4823 doi:10.1126/sciadv.aba4823

Ji, J., Chen, J., Balsam, W. L., Liu, L., Chen, Y., Zhao, L., et al. (2007). Quantitative Analysis of Hematite and Goethite in the Chinese Loess-Paleosol Sequences and its Implication for Dry and Humid Variability. *Quat. Sci.* 27, 221–229. doi:10.3321/j.issn:1001-7410.2007.02.007

Jiang, D., and Lang, X. (2010). Last Glacial Maximum East Asian Monsoon: Results of PMIP Simulations. *J. Clim.* 23, 5030–5038. doi:10.1175/2010jcli3526.1

Jo, K.-N., Woo, K. S., Yi, S., Yang, D. Y., Lim, H. S., Wang, Y., et al. (2014). Mid-latitude Interhemispheric Hydrologic Seesaw over the Past 550,000 Years. *Nature* 508, 378–382. doi:10.1038/nature13076

Kutzbach, J. E. (1981). Monsoon Climate of the Early Holocene: Climate Experiment with the Earth's Orbital Parameters for 9000 Years Ago. *Science* 214, 59–61. doi:10.1126/science.214.4516.59

Li, T., Liu, F., Abels, H. A., You, C.-F., Zhang, Z., Chen, J., et al. (2017). Continued Obliquity Pacing of East Asian Summer Precipitation after the Mid-pleistocene Transition. *Earth Planet. Sci. Lett.* 457, 181–190. doi:10.1016/j.epsl.2016.09.045

Lisiecki, L. E., and Raymo, M. E. (2005). A Pliocene-Pleistocene Stack of 57 Globally Distributed Benthic δ18O Records. *Paleoceanography* 20, a–n. doi:10.1029/2004PA001071

Liu, Z., Colin, C., Trentesaux, A., Blamart, D., Bassinot, F., Siani, G., et al. (2004). Erosional History of the Eastern Tibetan Plateau since 190 Kyr Ago: clay Mineralogical and Geochemical Investigations from the Southwestern South China Sea. *Mar. Geology.* 209, 1–18. doi:10.1016/j.margeo.2004.06.004

Lu, H., and An, Z. (1997). Paleoclimatic Significance of Grain Size Composite of Loess deposit in Luochuan. *Chin. Sci. Bull.* 42, 66–69. (In Chinese). doi:10.1007/BF02878745

Ma, L., Li, Y., Liu, X., and Sun, Y. (2017). Registration of Precession Signal in the Last Interglacial Paleosol (S 1) on the Chinese Loess Plateau. *Geochem. Geophys. Geosyst.* 18, 3964–3975. doi:10.1002/2017GC006964

Moore, D. M., and Reynolds, R. C. (1997). *X-Ray Diffraction and the Identification and Analysis of Clay Minerals*. New York, USA: Oxford University Press

Niu, D., Li, B., Wang, F., Wen, X., Ma, J., and Shu, P. (2015). Climate Changes Indicated by the clay Minerals: a Case of the Dishaogouwan Section on the southeastern Margin of the Mu Us Desert. *J. Fuzhou Univeristy (Natural Sci. Edition)* 43, 345–351.doi:10.7631/issn.1000-2243.2015.03.0345

Ortiz, J. D. (2011). Application of Visible/near Infrared Derivative Spectroscopy to Arctic Paleoceanography. *IOP Conf. Ser. Earth Environ. Sci.* 14. 012011 doi:10.1088/1755-1315/14/1/012011

Ortiz, J. D., O'connell, S. B., Delviscio, J., Dean, W., Carriquiry, J. D., Marchitto, T., et al. (2004). Enhanced marine Productivity off Western North America during Warm Climate Intervals of the Past 52 k.Y. *Geol* 32, 521–524. doi:10.1130/g20234.1

Ruddiman, W. F. (2006). What Is the Timing of Orbital-Scale Monsoon Changes. *Quat. Sci. Rev.* 25, 657–658. doi:10.1016/j.quascirev.2006.02.004

Shi, Z., Liu, X., and Cheng, X. (2012). Anti-phased Response of Northern and Southern East Asian Summer Precipitation to ENSO Modulation of Orbital Forcing. *Quat. Sci. Rev.* 40, 30–38. doi:10.1016/j.quascirev.2012.02.019

Shi, Z., Xie, X., Ren, X., Li, X., Yang, L., Lei, J., et al. (2019). Radiative Effect of Mineral Dust on East Asian Summer Monsoon during the Last Glacial Maximum: Role of Snow-Albedo Feedback. *Geophys. Res. Lett.* 46, 10901–10909. doi:10.1029/2019GL084211

Su, Q., Peng, C., Yi, L., Huang, H., Liu, Y., Xu, X., et al. (2016). An Improved Method of Sediment Grain Size Trend Analysis in the Xiaoqinghe Estuary, Southwestern Laizhou Bay, China. *Environ. Earth Sci.* 75, 1–10. doi:10.1007/s12665-016-5924-7

Sun, Y., He, L., Liang, L., and An, Z. (2011). Changing Color of Chinese Loess: Geochemical Constraint and Paleoclimatic Significance. *J. Asian Earth Sci.* 40, 1131–1138. doi:10.1016/j.jseaes.2010.08.006

Sun, Y., Yin, Q., Crucifix, M., Clemens, S. C., Araya-Melo, P., Liu, W., et al. (2019). Diverse Manifestations of the Mid-pleistocene Climate Transition. *Nat. Commun.* 10, 352. doi:10.1038/s41467-018-08257-9

Tan, L., Dong, G., An, Z., Lawrence Edwards, R., Li, H., Li, D., et al. (2021). Megadrought and Cultural Exchange along the Proto-Silk Road. *Sci. Bull.* 66, 603–611. doi:10.1016/j.scib.2020.10.011

Tan, L., Li, Y., Wang, X., Cai, Y., Lin, F., Cheng, H., et al. (2020). Holocene Monsoon Change and Abrupt Events on the Western Chinese Loess Plateau as Revealed by Accurately Dated Stalagmites. *Geophys. Res. Lett.* 47. e2020GL090273 doi:10.1029/2020GL090273

Tian, J., Zhao, Q., Wang, P., Li, Q., and Cheng, X. (2008). Astronomically Modulated Neogene Sediment Records from the South China Sea. *Paleoceanography* 23, a–n. doi:10.1029/2007pa001552

Wallace, J. M., and Hobb, P. V. (1977). *Atmospheric Science: An Introductory Survey*. New York: Academic Press .

Wang, B. (1994). Climatic Regimes of Tropical Convection and Rainfall. *J. Clim.* 7, 1109–1118. doi:10.1175/1520-0442(1994)007<1109:CROTCA>2.0.CO;2

Wang, B., and Ding, Q. (2008). Global Monsoon: Dominant Mode of Annual Variation in the Tropics. *Dyn. Atmospheres Oceans* 44, 165–183. doi:10.1016/j.dynatmoce.2007.05.002

Wang, P. (1999). Response of Western Pacific Marginal Seas to Glacial Cycles: Paleoceanographic and Sedimentological Features. *Mar. Geology.* 156, 5–39. doi:10.1016/S0025-3227(98)00172-8

Wang, P. X., Wang, B., Cheng, H., Fasullo, J., Guo, Z. T., Kiefer, T., et al. (2014). The Global Monsoon across Timescales: Coherent Variability of Regional Monsoons. *Clim. Past* 10, 2007–2052. doi:10.5194/cp-10-2007-2014

Wang, Y., Cheng, H., Edwards, R. L., He, Y., Kong, X., An, Z., et al. (2005). The Holocene Asian Monsoon: Links to Solar Changes and North Atlantic Climate. *Science* 308, 854–857. doi:10.1126/science.1106296

Wang, Y., Cheng, H., Edwards, R. L., Kong, X., Shao, X., Chen, S., et al. (2008). Millennial- and Orbital-Scale Changes in the East Asian Monsoon over the Past 224,000 Years. *Nature* 451, 1090–1093. doi:10.1038/nature06692

Wang, Y. J., Cheng, H., Edwards, R. L., An, Z., Wu, J., Chen, C.-C., et al. (2001). A High-Resolution Absolute-Dated Late Pleistocene Monsoon Record from Hulu Cave, China. *Science* 294, 2345–2348. doi:10.1126/science.1064618

Webster, P. J., Magaña, V. O., Palmer, T. N., Shukla, J., Tomas, R. A., Yanai, M., et al. (1998). Monsoons: Processes, Predictability, and the Prospects for Prediction. *J. Geophys. Res.* 103, 14451–14510. doi:10.1029/97jc02719

Xu, F., Hu, B., Zhao, J., Liu, X., Xu, K., Xiong, Z., et al. (2021). Provenance and Weathering of Sediments in the Deep basin of the Northern South China Sea during the Last 38 Kyr. *Mar. Geology.* 440. 106602 doi:10.1016/j.margeo.2021.106602

Yang, S., Ding, Z., Li, Y., Wang, X., Jiang, W., and Huang, X. (2015). Warming-induced Northwestward Migration of the East Asian Monsoon Rain belt from the Last Glacial Maximum to the Mid-holocene. *Proc. Natl. Acad. Sci. USA* 112, 13178–13183. doi:10.1073/pnas.1504688112

Yi, L., Chen, S., Ortiz, J. D., Chen, G., Peng, J., Liu, F., et al. (2016). 1500-year Cycle Dominated Holocene Dynamics of the Yellow River delta, China. *The Holocene* 26, 222–234. doi:10.1177/0959683615596834

Yi, L., Deng, C., Xu, X., Yu, H., Qiang, X., Jiang, X., et al. (2015). Paleo-megalake Termination in the Quaternary: Paleomagnetic and Water-Level Evidence from South Bohai Sea, China. *Sediment. Geology.* 319, 1–12. doi:10.1016/j.sedgeo.2015.01.005

Yi, L., Shi, Z., Tan, L., and Deng, C. (2018). Orbital-scale Nonlinear Response of East Asian Summer Monsoon to its Potential Driving Forces in the Late Quaternary. *Clim. Dyn.* 50, 2183–2197. doi:10.1007/s00382-017-3743-5

Yi, L., Yu, H.-J., Ortiz, J. D., Xu, X.-Y., Chen, S.-L., Ge, J.-Y., et al. (2012a). Late Quaternary Linkage of Sedimentary Records to Three Astronomical Rhythms and the Asian Monsoon, Inferred from a Coastal Borehole in the South Bohai Sea, China. *Palaeogeogr. Palaeoclimatol. Palaeoecol.* 329-330, 101–117. doi:10.1016/j.palaeo.2012.02.020

Yi, L., Yu, H., Ortiz, J. D., Xu, X., Qiang, X., Huang, H., et al. (2012b). A Reconstruction of Late Pleistocene Relative Sea Level in the South Bohai Sea, China, Based on Sediment Grain-Size Analysis. *Sediment. Geology.* 281, 88–100. doi:10.1016/j.sedgeo.2012.08.007

Yuan, D., Cheng, H., Edwards, R. L., Dykoski, C. A., Kelly, M. J., Zhang, M., et al. (2004). Timing, Duration, and Transitions of the Last Interglacial Asian Monsoon. *Science* 304, 575–578. doi:10.1126/science.1091220

Zhang, H., Brahim, Y., Li, H., Zhao, J., Kathayat, G., Tian, Y., et al. (2019). The Asian Summer Monsoon: Teleconnections and Forcing Mechanisms-A Review from Chinese Speleothem δ18O Records. *Quaternary* 2, 26. doi:10.3390/quat2030026

Zhang, H., Zhang, X., Cai, Y., Sinha, A., Spötl, C., Baker, J., et al. (2021). A Data-Model Comparison Pinpoints Holocene Spatiotemporal Pattern of East Asian Summer Monsoon. *Quat. Sci. Rev.* 261. 106911 doi:10.1016/j.quascirev.2021.106911

Zhang, P., Cheng, H., Edwards, R. L., Chen, F., Wang, Y., Yang, X., et al. (2008). A Test of Climate, Sun, and Culture Relationships from an 1810-Year Chinese Cave Record. *Science* 322, 940–942. doi:10.1126/science.1163965

Zhao, H., Sun, Y., and Qiang, X. (2017). Iron Oxide Characteristics of Mid-miocene Red Clay Deposits on the Western Chinese Loess Plateau and Their Paleoclimatic Implications. *Palaeogeogr. Palaeoclimatol. Palaeoecol.* 468, 162–172. doi:10.1016/j.palaeo.2016.12.008

Zhisheng, A., Clemens, S. C., Shen, J., Qiang, X., Jin, Z., Sun, Y., et al. (2011). Glacial-Interglacial Indian Summer Monsoon Dynamics. *Science* 333, 719–723. doi:10.1126/science.1203752

Zhisheng, A., Guoxiong, W., Jianping, L., Youbin, S., Yimin, L., Weijian, Z., et al. (2015). Global Monsoon Dynamics and Climate Change. *Annu. Rev. Earth Planet. Sci.* 43, 29–77. doi:10.1146/annurev-earth-060313-054623

Zhisheng, A., Kutzbach, J. E., Prell, W. L., and Porter, S. C. (2001). Evolution of Asian Monsoons and Phased Uplift of the Himalaya-Tibetan Plateau since Late Miocene Times. *Nature* 411, 62–66. doi:10.1038/35075035

Zhou, X., Liu, Z., Yan, Q., Zhang, X., Yi, L., Yang, W., et al. (2019). Enhanced Tropical Cyclone Intensity in the Western North Pacific during Warm Periods over the Last Two Millennia. *Geophys. Res. Lett.* 46, 9145–9153. doi:10.1029/2019GL083504

Conflict of Interest: The authors declare that the research was conducted in the absence of any commercial or financial relationships that could be construed as a potential conflict of interest.

Publisher's Note: All claims expressed in this article are solely those of the authors and do not necessarily represent those of their affiliated organizations, or those of the publisher, the editors and the reviewers. Any product that may be evaluated in this article, or claim that may be made by its manufacturer, is not guaranteed or endorsed by the publisher.